

Roads for right-handed neutrino dark matter: Fast expansion, standard freeze-out, and early matter domination

Giorgio Arcadi,^{1,2,3,*} Jacinto Paulo Neto^{4,5,†} Farinaldo S. Queiroz,^{4,5,6,‡} and Clarissa Siqueira^{7,§}

¹*Dipartimento di Matematica e Fisica, Università di Roma Tre, Via della Vasca Navale 84, 00146 Rome, Italy*

²*INFN Sezione di Roma Tre, Via della Vasca Navale 84, 00146 Rome, Italy*

³*Dipartimento di Scienze Matematiche e Informatiche, Scienze Fisiche e Scienze della Terra, Università degli Studi di Messina, Via Ferdinando Stagno d'Alcontres 31, I-98166 Messina, Italy*

⁴*Departamento de Física, Universidade Federal do Rio Grande do Norte, 59078-970 Natal, RN, Brasil*

⁵*International Institute of Physics, Universidade Federal do Rio Grande do Norte, Campus Universitário, Lagoa Nova, Natal-RN 59078-970, Brazil*

⁶*Millennium Institute for Subatomic Physics at High-Energy Frontier (SAPHIR), Fernandez Concha 700, Santiago 7550196, Chile*

⁷*Instituto de Física de São Carlos, Universidade de São Paulo, Avenida Trabalhador São-carlense, 400, São Carlos-SP, 13566-590, Brazil*



(Received 6 September 2021; accepted 25 January 2022; published 15 February 2022)

Right-handed neutrinos appear in several extensions beyond the Standard Model, especially in connection to neutrino masses. Motivated by this, we present a model of right-handed neutrino dark matter that interacts with Standard Model particles through a new gauge symmetry as well as via mass mixing between the new vector field and the Z boson, and investigate different production mechanisms. We derive the dark matter relic density when the Hubble rate is faster than usual, when dark matter decouples in a matter domination epoch, and when it decouples in a radiation domination regime, which is then followed by a matter domination era. The direct detection rate features a spin-independent but velocity suppressed operator, as well as a spin-dependent operator when the mass mixing is correctly accounted for. We put all these results into perspective with existing flavor physics, atomic parity violation, and collider bounds. Lastly, we outline the region of parameter space in which weak-scale right-handed neutrino dark matter stands as a viable dark matter candidate.

DOI: [10.1103/PhysRevD.105.035016](https://doi.org/10.1103/PhysRevD.105.035016)

I. INTRODUCTION

The presence of dark matter in our Universe is ascertained through a variety of datasets, from dwarf galaxy scales to cosmological scales. The precision acquired by cosmic microwave background (CMB) probes allowed us to quantify precisely the abundance of dark matter in our Universe. Dark matter accounts for nearly 27% of the total energy density [1]. Its nature is unknown, though. Massive particles that feature weak interactions with Standard Model (SM) particles, dubbed (WIMPs), have stood out from the crowd, driving most experimental efforts for many

years [2]. Currently, other plausible dark matter candidates such as the axion and axionlike particles, which have always been theoretically compelling, gained lots of interest from the community due to the nonpositive signals in WIMP searches [3]. However, no solid positive signals have been observed favoring other dark matter candidates either. The customary assumption that dark matter had a thermal production has given us a misapprehension that a positive signal should appear in the current generation of experiments. There are ways to successfully have a thermal dark matter candidate while yielding no signal at current direct detection experiments. Hence, this sudden disbelief for the WIMP miracle does not seem justified. It has always been worthwhile to explore well-motivated dark matter production mechanisms that lead to attainable detection, especially if the mechanism still leaves imprints at current experiments.

Besides the dark matter siege, neutrino masses stand as concrete evidence for physics beyond the Standard Model. With the observation of neutrino oscillations, we have concluded that at least two neutrinos are massive [4–11].

*giorgio.arcadi@uniroma3.it
 †jacinto.neto.100@ufrn.edu.br
 ‡farinaldo.queiroz@iip.ufrn.br
 §csiqueira@ifsc.usp.br

Published by the American Physical Society under the terms of the [Creative Commons Attribution 4.0 International license](https://creativecommons.org/licenses/by/4.0/). Further distribution of this work must maintain attribution to the author(s) and the published article's title, journal citation, and DOI. Funded by SCOAP³.

It should be noted that the sum of the neutrino masses is constrained by CMB observations because the energy density of neutrinos, which depends on the sum of neutrino masses, affects both the relativistic and nonrelativistic energy density relevant to the derivation of the CMB temperature and polarization power spectra [12]. In fact, CMB probes give rise to the most stringent bound which reads $\Sigma m_\nu < 0.12$ eV [13]. However, the individual masses are unknown.

An elegant solution to theoretically generate neutrino masses is offered by right-handed neutrinos. In particular, if copies of right-handed neutrinos are added to the Standard Model, one can naturally address neutrino masses through a type I seesaw mechanism when both Dirac and Majorana mass terms are included in the Yukawa Lagrangian. The Majorana mass is expected to be very large to play the seesaw and bring the active neutrino masses down below the eV scale.

That said, one may wonder if the mechanisms behind the presence of dark matter in our Universe are somehow connected to neutrino masses. This question has driven a multitude of works. In particular, we will be interested in connecting these two new physics landmarks in the context of the type I seesaw mechanism [14–28], which features the Lagrangian

$$\mathcal{L} \supset y_{ab} \overline{L}_a \Phi N_{bR} + \frac{M_a}{2} \overline{N}_{aR}^c N_{aR}, \quad (1)$$

where Φ is the SM Higgs doublet, and M is the Majorana mass term for the right-handed neutrinos. Note that this Majorana mass is a 3×3 matrix. After spontaneous electroweak symmetry breaking, the first term yields a Dirac mass term for the active neutrinos. The presence of a Majorana mass allow us to employ the so-called type I seesaw mechanism that results into $m_\nu \simeq m_D^T M^{-1} m_D$ and $m_N \sim M$.

For Yukawa couplings of order one in Eq. (1), this simple and plausible framework requires the right-handed neutrino masses to be very large—above 10^{12} GeV. Consequently, this mechanism is hardly testable by existing experiments. It would be interesting if one could successfully explain neutrino masses and dark matter without invoking a very large energy scale suppression. A possible route is to consider light right-handed neutrinos with masses around 1 keV. If one of the three right-handed neutrinos is lighter than the others, then it can be made cosmologically stable as long as the mixing between active and right-handed neutrinos is sufficiently small. This scenario is dubbed sterile neutrino dark matter [29,30].¹ The dark matter relic density is found through a nonresonant production [29], which is based on the active-sterile neutrino oscillations. The approximate relic density is [32–36]

$$\Omega_N h^2 \sim 0.1 \left(\frac{\sin^2 \theta_i}{3 \times 10^{-9}} \right) \left(\frac{m_N}{3 \text{ keV}} \right)^{1.8}, \quad (2)$$

where $\sin^2 \theta_i \sim \sum_a y_{ab}^2 v^2 / M^2$ is the active-sterile neutrino mixing and v is the SM Higgs vacuum expectation value. As mentioned earlier, the sterile neutrino is unstable because of its mixing with the active neutrinos. In fact, this mixing leads to the decays $N \rightarrow \nu \nu \nu$ and $N \rightarrow \nu \gamma$ [37,38]. The latter decay has been extensively looked for in x-ray surveys. However, such x-ray searches combined with structure formation requirements rule out this sterile neutrino production [39,40]. There are ways to bypass this exclusion by evoking other production mechanisms [41,42]. Instead of dwelling on light sterile neutrinos as dark matter, we investigate under which circumstance we can accommodate the type I seesaw mechanism, while hosting a TeV scale right-handed neutrino dark matter. Note that we have renamed sterile neutrino as right-handed neutrino. Theoretically speaking, they are the same field, but when one refers to sterile neutrinos small masses and suppressed mixing angles are typically adopted. When these sterile neutrinos are heavy, with masses above 1 MeV, the term right-handed neutrino is used more often.²

Anyway, how can we have a weak-scale right-handed neutrino dark matter have the presence of the first term in Eq. (1), which is necessary for the type-I seesaw to work, but make it unstable? The idea is to invoke a \mathcal{Z}_2 symmetry, where only one of the right-handed neutrinos is odd under it [45–48]. In this way, two massive right-handed neutrinos will play a role in the seesaw mechanism, whereas the lightest becomes a plausible dark matter candidate. In absence of a symmetry one should invoke a fine-tuned suppression of the Yukawa couplings to make the right-handed neutrino a viable DM candidate. We focus on the latter. Similar works have been carried out in this direction [49–51]. However, our work extends previous studies because we go beyond the standard freeze-out case. Concretely, we investigate the right-handed neutrino dark matter scenario under three different cosmological histories, namely fast expansion, matter domination during freeze-out, and matter domination after freeze-out. These cosmological histories change the theoretical predictions for the dark matter relic density compared to the standard freeze-out case, and consequently lead to different conclusions. Besides computing the dark matter relic density under different cosmological scenarios, we also compute the dark matter scattering cross section. We highlight that for right-handed neutrino dark matter, the dark matter scattering cross section does not fall into the standard classification of spin-independent or spin-dependent dark-matter-nucleon scattering. Therefore, we need to compare the resulting scattering rate with the data to derive the

¹For a sterile neutrino and Higgs portal considering a freeze-in production mechanism, see [31].

²We can also find heavy right-handed neutrinos in an asymmetric dark matter scenario [43,44].

correct limits. Lastly, we also include collider bounds on the mediator masses based on the LHC search for heavy dilepton resonances.

All of this procedure is done in a well-motivated two Higgs doublet model (2HDM) featuring an Abelian gauge symmetry, a model that can elegantly solve the flavor problem present in general 2HDM constructions, and address neutrino masses via the type I seesaw mechanism. 2HDMs featuring new gauge symmetries are increasingly getting interest from the community because they offers new collider signatures [50,52–55] and avenues to be explored concerning atomic parity violation [56,57], neutrino-electron scattering [58], axionlike particles [59], exotic Higgs decays [60–62], neutrino masses [63–65], flavor studies [66–69], and dark matter [15,70–75], among others [76–80]. Hence, it is definitely worthwhile to investigate how feasible it is to host a dark matter candidate connected to neutrino masses and cosmological histories that go beyond the standard freeze-out.

II. THE MODEL

2HDMs have been extensively studied in the literature [81–83] for naturally keeping the ρ parameter unchanged despite the extended scalar sector. Furthermore, it leads to interesting collider searches that are within reach of the LHC. However, the canonical version of the 2HDM suffers from flavor changing neutral interactions and does not address neutrino masses. It would be appealing if one could solve both issues via gauge symmetries. This is precisely the idea behind the 2HDM-U(1). An Abelian gauge symmetry is incorporated to the 2HDM in such a way that only one scalar doublet contributes to fermion masses, and three right-handed neutrinos are required to cancel the gauge anomalies and consequently play a role in the type I seesaw mechanism aforementioned. We will choose the new Abelian gauge symmetry to be the baryon-lepton ($B - L$) number, for concreteness, but we highlight that other gauge symmetries are also conceivable. The purpose of our work is to incorporate dark matter without adding new fields and explore the impact of our conclusions under different cosmological histories. Concerning the model itself, which is based on the $SU(3)_c \times SU(2)_L \times U(1)_Y \times U(1)_{B-L}$, the fermion content features

$$Q_{aL} = \begin{pmatrix} u_{aL} \\ d_{aL} \end{pmatrix} \sim (\mathbf{3}, \mathbf{2}, 1/6, 1/3),$$

$$u_{aR} \sim (\mathbf{3}, \mathbf{1}, 2/3, 1/3) \quad \text{and} \quad d_{aR} \sim (\mathbf{3}, \mathbf{1}, -1/3, 1/3),$$

and

$$L_{aL} = \begin{pmatrix} e_{aL} \\ \nu_{aL} \end{pmatrix} \sim (\mathbf{1}, \mathbf{2}, -1/2, -1),$$

$$e_{aR} \sim (\mathbf{1}, \mathbf{1}, -1, -1) \quad \text{and} \quad N_{aR} \sim (\mathbf{1}, \mathbf{1}, 0, -1).$$

Notice that thus far the only difference to the SM is the presence of right-handed neutrinos. The model has three scalar fields,

$$\Phi_1 = \begin{pmatrix} \phi_1^+ \\ \phi_1^0 \end{pmatrix} \sim (\mathbf{1}, \mathbf{2}, 1/2, 2), \quad (3)$$

$$\Phi_2 = \begin{pmatrix} \phi_2^+ \\ \phi_2^0 \end{pmatrix} \sim (\mathbf{1}, \mathbf{2}, 1/2, 0), \quad (4)$$

and

$$\Phi_s \sim (\mathbf{1}, \mathbf{1}, 0, 2),$$

where the subscript $a = 1, 2, 3$ accounts for the three generations. We stress that the presence of the scalar singlet is twofold: (i) it breaks the U(1) gauge symmetry generating mass to the Z' gauge boson; (ii) it gives rise to the Majorana mass for the right-handed neutrinos. In the original version of the type I seesaw, we have a Majorana bare mass term for the right-handed neutrino masses, but in our work it is generated through a mechanism of spontaneous symmetry breaking. This fact will be clear below. Fermions get mass through the Yukawa Lagrangian $\mathcal{L}_Y = \mathcal{L}_{Y_1} + \mathcal{L}_{Y_2}$, where

$$\mathcal{L}_{Y_1} = -y_{ab}^d \bar{Q}_a \Phi_1 d_{bR} - y_{ab}^u \bar{Q}_a \tilde{\Phi}_1 u_{bR} - y_{ab}^e \bar{L}_a \Phi_1 e_{bR} + \text{H.c.}, \quad (5)$$

and

$$\mathcal{L}_{Y_2} \supset -y_{ab} \bar{L}_a \tilde{\Phi}_2 N_{bR} - y_{ab}^M \overline{(N_{aR})^c} \Phi_s N_{bR}. \quad (6)$$

Having a weak-scale right-handed neutrino from Eq. (6) requires the addition of an extra discrete symmetry. We will invoke a \mathcal{Z}_2 symmetry to stabilize, say N_{1R} , the lightest right-handed neutrino. In this way, the first term in Eq. (6) involves only two right-handed neutrinos, whereas the latter remains unaltered as long as y_{ij}^M is diagonal. The two right-handed neutrinos in the Dirac mass term act the type I seesaw mechanism leading to two massive active neutrinos and a massless one, in agreement with neutrino oscillation observations [84]. This is a well-known fact which can be directly seen using the Casas-Ibarra parametrization where the neutrino masses are directly tied to the Yukawa couplings. As we are basically removing one Yukawa coupling, the first term of Eq. (6), which is a 6×6 matrix, should have at least four nonzero entries. Using the Casas-Ibarra parametrization one can see that the Yukawa matrix will depend on two right-handed neutrino masses and two active neutrino masses [85]. We emphasize that we have assumed that the Majorana mass matrix is purely diagonal.

The scalar potential, in agreement with the gauge charges of the doublets, including the singlet scalar, is given by

$$\begin{aligned}
 V(\Phi_{1,2,s}) &= m_{11}^2 \Phi_1^\dagger \Phi_1 + m_{22}^2 \Phi_2^\dagger \Phi_2 + m_s^2 \Phi_s^\dagger \Phi_s \\
 &+ \frac{\lambda_1}{2} (\Phi_1^\dagger \Phi_1)^2 + \frac{\lambda_2}{2} (\Phi_2^\dagger \Phi_2)^2 + \frac{\lambda_s}{2} (\Phi_s^\dagger \Phi_s)^2 \\
 &+ \lambda_3 (\Phi_1^\dagger \Phi_1) (\Phi_2^\dagger \Phi_2) + \lambda_4 (\Phi_1^\dagger \Phi_2) (\Phi_2^\dagger \Phi_1) \\
 &+ \mu_1 \Phi_1^\dagger \Phi_1 \Phi_s^\dagger \Phi_s + \mu_2 \Phi_2^\dagger \Phi_2 \Phi_s^\dagger \Phi_s \\
 &+ (\mu \Phi_1^\dagger \Phi_2 \Phi_s + \text{H.c.}). \tag{7}
 \end{aligned}$$

The neutral components of all scalars acquire vacuum expectation values (VEVs) as

$$\Phi_i = \frac{1}{\sqrt{2}} (v_i + \rho_i + i\eta_i), \tag{8}$$

and

$$\Phi_s = \frac{1}{\sqrt{2}} (v_s + \rho_s + i\eta_s),$$

which give mass to all fermions and gauge bosons. It is important to emphasize that the dark matter candidate N_{1R} becomes massive through the singlet scalar VEV, v_s ,

$$m_N = \frac{y_N^M}{\sqrt{2}} v_s. \tag{9}$$

Concerning the gauge sector, kinetic mixing arises at tree-level,

$$\mathcal{L}_{\text{gauge}} = -\frac{1}{4} \hat{B}_{\mu\nu} \hat{B}^{\mu\nu} + \frac{\epsilon}{2 \cos \theta_W} \hat{X}_{\mu\nu} \hat{B}^{\mu\nu} - \frac{1}{4} \hat{X}_{\mu\nu} \hat{X}^{\mu\nu}, \tag{10}$$

with ϵ , the kinetic mixing parameter, and θ_W , the Weinberg angle. The Lagrangian responsible for gauge bosons' masses is given by

$$\mathcal{L} = (D^\mu \phi_1)^\dagger (D_\mu \phi_1) + (D^\mu \phi_2)^\dagger (D_\mu \phi_2) + (D^\mu \phi_s)^\dagger (D_\mu \phi_s), \tag{11}$$

where the covariant derivative is

$$D_\mu = \partial_\mu + igT^a W_\mu^a + ig' \frac{Q_Y}{2} \hat{B}_\mu + ig_X \frac{Q_X}{2} \hat{X}_\mu, \tag{12}$$

with Q_Y and Q_X being the charges under Yukawa and $B-L$ gauge symmetries, respectively, g and g' being the usual gauge couplings associated with $SU(2)_L$ and $U(1)_Y$ symmetries, respectively, and g_X , the $B-L$ coupling. Diagonalizing the matrices for X_μ and Z_μ bosons (for details we recommend [71]), we get the following gauge boson masses:

$$m_W^2 = \frac{1}{4} g^2 v^2, \tag{13}$$

$$m_Z^2 = \frac{1}{4} g_Z^2 v^2, \tag{14}$$

$$m_{Z'}^2 = g_X^2 v_s^2 + g_X^2 v^2 \cos^2 \beta \sin^2 \beta, \tag{15}$$

where $v^2 = v_1^2 + v_2^2 = 246^2 \text{ GeV}^2$ and $g_Z = g/\cos \theta_W$. The Lagrangian in Eq. (11) is also responsible for the interactions between gauge bosons and scalars, for example $Z'W^+W^-$, $Z'W^+H^-$, $HZ'Z'$, $hZ'Z'$, HZZ' , which are also relevant for the dark matter phenomenology. These couplings can be found in [71]. We emphasize that we have taken the kinetic mixing to be zero at tree-level. At the one-loop level, it can be safely ignored, as our phenomenology will be driven by the gauge coupling g_X .

The dark matter phenomenology of the model is governed by the neutral current involving the Z and Z' gauge bosons that read [49,86]

$$\begin{aligned}
 \mathcal{L}_{\text{NC}} &= -eJ_{em}^\mu A_\mu - \frac{g}{2 \cos \theta_W} J_{\text{NC}}^\mu Z_\mu \\
 &- \left(eeJ_{em}^\mu + \frac{\epsilon_Z g}{2 \cos \theta_W} J_{\text{NC}}^\mu \right) Z'_\mu \\
 &- \frac{g_X}{2} Q_{X_f} (\bar{\psi}_f \gamma^\mu \psi_f) Z'_\mu \\
 &+ \frac{1}{4} g_X (N_{1R} \gamma^\mu \gamma_5 N_{1R}) Z'_\mu,
 \end{aligned}$$

where $Q_{X_f} = -1$ for charged leptons, $Q_{X_f} = 1/3$ for quarks, and where

$$\epsilon_Z \equiv \frac{2g_X}{g_Z} \cos^2 \beta, \tag{16}$$

and

$$J_{\text{NC}}^\mu = (T_{3f} - 2Q_{Yf} \sin^2 \theta_W) \bar{\psi}_f \gamma^\mu \psi_f - T_{3f} \bar{\psi}_f \gamma^\mu \gamma_5 \psi_f. \tag{17}$$

Identifying N_{1R} as our dark matter candidate, we can straightforwardly carry out the dark matter phenomenology within the standard freeze-out and Λ CDM model. This scenario was investigated somewhere else, Ref. [71]. Our plan is to go beyond and explore other cosmological scenarios. To do so, we start by reviewing the important ingredients of dark energylike early radiation, and early matter domination epochs. We have now set the particle physics model, and we will review the cosmological background.

III. NONSTANDARD COSMOLOGY HISTORIES

In this section, we explore how the dark matter relic density may be affected by a nonstandard cosmological history, where the right-handed neutrino dark matter candidate decouples from thermal equilibrium in different scenarios. The key aspect of different cosmology histories is the

effect on the Hubble expansion rate, because it directly impacts the Boltzmann equations. The Hubble rate evolves differently for matter, radiation, and dark energylike fields. Thus, depending on which component dominates H , distinct solutions to the dark matter relic abundance are found.

The standard cosmology predicts that the Universe is radiation dominated at early times. However, before the big bang nucleosynthesis (BBN), we have the freedom to choose different cosmological histories for short period of times. For example, the expansion rate may be governed by matter or a new field, which leads to a faster expansion rate. That said, we tease out the dark matter phenomenology when the dark matter particles decouples during (i) an expansion rate faster than radiation (Sec. III A); (ii) a radiation-dominated era, early radiation domination (ERD), followed by a matter-dominated period (Sec. III B); and (iii) in a matter-dominated phase, early matter domination (EMD) (Sec. III C). We start reviewing the key ingredients of a faster expansion episode and how it changes the Boltzmann equation.

A. Faster than usual early expansion

We assume that a new scalar field ϕ has an energy density that grows with the scale factor as

$$\rho_\phi(t) \propto a(t)^{-(4+n)}, \quad n > 0, \quad (18)$$

where n encodes the nonstandard cosmological evolution. Notice that for $n = 0$, we recover the radiation energy density $\rho_R(t) \propto a(t)^{-4}$ that corresponds to the standard case. Then, the scalar field energy density ρ_ϕ dominates over radiation at early times and redshifts faster than usual as the universe expands.

Let us start by assuming that at some period of the early Universe, the Hubble expansion rate was driven by radiation and ϕ energy densities. Thus, the total energy density can be written as

$$\rho = \rho_R + \rho_\phi. \quad (19)$$

Nevertheless, the radiation energy density ρ_R must overcome ρ_ϕ at a time before BBN to avoid any tension with observations [87]. Then, we define the temperature T_r at which $\rho_R(T_r) = \rho_\phi(T_r)$. To be consistent with BBN observations, we impose

$$T_r \gtrsim (15.4)^{1/n} \text{ MeV}. \quad (20)$$

When the scalar energy density ρ_ϕ is negligible, the radiation energy density evolves with the temperature as usual, with

$$\rho_R(T) = \frac{\pi^2}{30} g_\star(T) T^4, \quad (21)$$

where $g_\star(T)$ is the effective number of relativistic degrees of freedom at temperature T .

The next step is to express the energy density of ϕ in terms of temperature. Firstly, it is important to remember that the entropy density is given by

$$s(T) = \frac{2\pi^2}{45} g_{\star s}(T) T^3, \quad (22)$$

where $g_{\star s}(T)$ is the effective degrees of freedom of the SM entropy density. Using entropy conservation per comoving volume, $sa^3 = \text{const.}$, we get,

$$a(T) \propto (g_\star^{1/3}(T) T)^{-1}. \quad (23)$$

Inserting this result into Eq. (18), and taking the ratio $\rho_\phi(T)/\rho_\phi(T_r)$, the ϕ energy density can be written as a function of temperature as

$$\rho_\phi(T) = \rho_\phi(T_r) \left(\frac{g_{\star s}(T)}{g_{\star s}(T_r)} \right)^{(4+n)/3} \left(\frac{T}{T_r} \right)^{4+n}. \quad (24)$$

Finally, using the definition $\rho_R(T_r) = \rho_\phi(T_r)$, the total energy density at temperature $T > T_r$ becomes

$$\begin{aligned} \rho(T) &= \rho_R(T) + \rho_\phi(T) \\ &= \rho_R(T) \left[1 + \frac{g_\star(T_r)}{g_\star(T)} \left(\frac{g_{\star s}(T)}{g_{\star s}(T_r)} \right)^{(4+n)/3} \left(\frac{T}{T_r} \right)^n \right]. \end{aligned} \quad (25)$$

From this equation, we conclude that ϕ dominates the universe for temperatures $T \gtrsim T_r$.

Once we know the evolution of the energy density, we can determine the Hubble rate using the Friedmann equation [88],

$$H = \sqrt{\frac{\rho}{3M_{\text{Pl}}^2}}, \quad (26)$$

where $M_{\text{Pl}} = (8\pi G)^{-1/2} = 2.4 \times 10^{18} \text{ GeV}$. Assuming that $g_\star(T) = g_\star$ is a constant for temperatures $T \gg T_r$, i.e., for the period in which ρ_ϕ completely dominates over ρ_R , the Hubble rate becomes [87]

$$H(T) \approx \frac{\pi}{3} \sqrt{\frac{g_\star}{10 M_{\text{Pl}}}} \left(\frac{T}{T_r} \right)^{n/2}, \quad (27)$$

with $g_\star = 106.75$ accounting for the entire SM degrees of freedom. Knowing the Hubble rate in the Λ CDM radiation-dominated cosmology [89],

$$H_R(T) = \frac{\pi}{3} \sqrt{\frac{g_\star}{10 M_{\text{Pl}}}} T^2, \quad (28)$$

we can rewrite Eq. (27) as

$$H(T) \approx H_R(T) \left(\frac{T}{T_r} \right)^{n/2}, \quad (29)$$

where we can explicitly see that for temperatures $T > T_r$, nonstandard cosmologies ($n > 0$) make the Universe expand faster than in the standard radiation-dominated epoch. Setting T_f to be the freeze-out temperature, having a dark matter particle freezing out in a fast expanding universe requires $T_f > T_{frad}$. Note that from our reasoning for temperatures larger than T_r , a nonstandard cosmology is at play.

With Eq. (27) at hand, we can compute the dark matter relic abundance for the right-handed neutrino N_{1R} when the universe expands too fast. In the standard radiation-dominated scenario, the Boltzmann equation that describes the evolution of the comoving dark matter number density $Y_N \equiv n_N/s$ is

$$\frac{dY_N}{dx} = -\frac{s\langle\sigma v\rangle}{H(x)x} (Y_N^2 - Y_N^{\text{eq}2}), \quad (30)$$

with $x \equiv m_N/T$ and $\langle\sigma v\rangle$ being the thermally averaged annihilation cross section, and $H(x)$ the standard radiation-dominated Hubble rate. The comoving equilibrium number density can be written as a function of x for a Maxwell-Boltzmann distribution as follows [87]:

$$Y_N^{\text{eq}}(x) = \frac{45g_N}{4\pi^4 g_{\star s}} x^2 K_2(x), \quad (31)$$

where g_N accounts for the degrees of freedom of the right-handed neutrino dark matter and $K_2(x)$ is the modified Bessel function. With $x_r = m_N/T_r$ and $x_f = m_N/T_f$, we obtain

$$H(x) \simeq \frac{\pi}{3} \sqrt{\frac{g_{\star}}{10}} \frac{m_N^2}{M_{\text{Pl}}} x^{-2} \left(\frac{x_r}{x} \right)^{n/2}, \quad (32)$$

and then from Eq. (30) we find

$$\frac{dY_N}{dx} = -\frac{A\langle\sigma v\rangle}{x^{2-n/2}(x^n + x_r^n)^{1/2}} (Y_N^2 - Y_N^{\text{eq}2}), \quad (33)$$

where $A = \frac{2\sqrt{2}\pi}{3\sqrt{5}} g_{\star}^{1/2} M_{\text{Pl}} m_N$. Approximate analytical solutions are given by [87]

$$Y_N(x) \simeq \frac{x_r}{m_N M_{\text{Pl}} \langle\sigma v\rangle} \left[\frac{2}{x_f} + \log\left(\frac{x}{x_f}\right) \right]^{-1}, \quad n = 2$$

$$Y_N(x) \simeq \frac{x_r^{n/2}}{2m_N M_{\text{Pl}} \langle\sigma v\rangle} \left[x_f^{n/2-2} + \frac{x^{n/2-1}}{n-1} \right]^{-1}, \quad n > 2. \quad (34)$$

Equations (34) are valid for s -wave annihilation processes. In other words, when $\langle\sigma v\rangle$ does not depend on temperature. Thus, these approximate analytical solutions can only be

extrapolated up to $x = x_r$. In Fig. 1, we present the numerical result for the yield, assuming the dark matter mass $m_N = 100$ GeV and the annihilation cross section $\langle\sigma v\rangle = 10^{-9}$ GeV $^{-2}$, for the following values of $T_r = 0.1$ GeV (brown line), $T_r = 1$ GeV (blue line), $T_r = 10$ GeV (red line), and $n = 4$. For completeness, we also include the yield for the standard case (black line).

The $n > 0$ cosmologies can produce a higher comoving dark matter number density at the time of freeze-out, $x_f < x_r$. However, for the s -wave annihilation cross section and $n \geq 2$, the annihilation rate after freeze-out scales as $\Gamma \propto T^3$, whereas $H \propto T^{2+n/2}$. Hence, the annihilation rate redshifts either slower than (or equally to) the Hubble rate. Consequently, after freeze-out the dark matter keeps annihilating until the temperature T_r , i.e., until radiation starts to govern the universe expansion. In this epoch, $H_R \propto T^2$, meaning that the dark matter will stop annihilating, leading to a constant energy density.

In Fig. 2, we briefly illustrate the thermal history for the $n \geq 2$ cosmologies. The dark matter decouples at T_f while the scalar field dominates. The period $T_r < T < T_f$ defines the *relentless* phase in which the dark matter tries relentlessly to go back to thermal equilibrium, unsuccessfully [87]. For $n = 2$, Eq. (34) translates the relentless effect via the slow logarithmic decrease of the comoving dark matter number density. Although for $n > 2$, the comoving dark matter number density decreases following a power law.

Finally, solving Eq. (33) numerically, we compute the dark matter relic density taking $x \rightarrow \infty$ via the following expression:

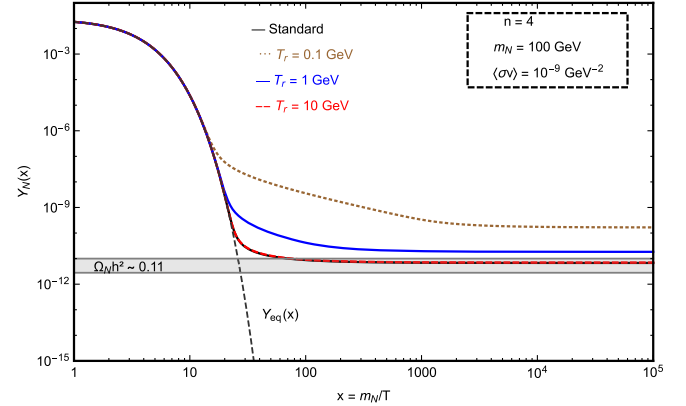


FIG. 1. We exhibit of the yield *versus* x for a freeze-out happening during the fast expansion regime. For this case, we choose the dark matter mass $m_N = 100$ GeV and the annihilation cross section $\langle\sigma v\rangle = 10^{-9}$ GeV $^{-2}$ for the following values of $T_r = 0.1$ (brown line), $T_r = 1$ GeV (blue line), $T_r = 10$ GeV (red line), and $n = 4$. For completeness, we also include the yield for the standard case (black line). Note that for $T_r = 10$ GeV, we have a superposition with the standard case. The shaded gray region is the approximate range for the correct dark matter relic abundance as measured by Planck [13]. It is clear that the longer the period of ϕ dominance, the larger the impact on the yield.

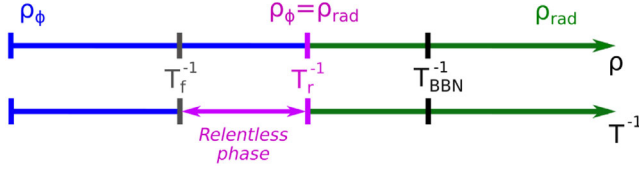


FIG. 2. Illustration of the density energy evolution and thermal history for *faster early expansion than usual cosmologies*.

$$\begin{aligned}\Omega_N h^2 &= \frac{s_0}{\rho_0} h^2 m_N Y_N(x \rightarrow \infty) \\ &\simeq 2.82 \times 10^8 m_N Y_N(x \rightarrow \infty),\end{aligned}\quad (35)$$

where s_0 stands for the SM entropy density today, ρ_0 the critical energy density, and h is the scale factor for the Hubble expansion rate [90].

In summary, our dark matter phenomenology is ruled by five free parameters. They encode the interplay between particle physics and cosmology, namely the new gauge coupling, g_X , the dark matter mass, m_N , the mediator mass, $m_{Z'}$, and the (n, T_r) , which are the cosmological input parameters that are related to the energy density of the scalar field that eventually governs the expansion rate of the universe.

We emphasize that the key cosmological input here is the energy density of the scalar field. It suffices to determine (n, T_r) and thus describe the entire background in which the dark matter was thermally produced [87]. However, many single scalar field cosmologies can reproduce the behavior in Eq. (25). For $n = 2$, with positive scalar potential, it is associated to theories of *quintessence* fluids. In our work, we will assume that the energy density scales as $\rho_\phi \propto a^{-6}$ in the kination regime [91–93]. Also, Chaplyng gas theories can reproduce the redshift behavior in Eq. (25) and possibly explain dark matter and dark energy [94,95]. Although, for $n > 2$, the theories with negative scalar potentials are needed [87,96].

B. Freeze-out during early radiation-dominated era followed by a matter domination period

In a similar vein, we assume the existence of a scalar field ϕ that dominates the Hubble expansion rate during some period in the early Universe before its decay into SM radiation. However, at this time, ϕ behaves as a pressureless fluid.³ After ϕ decay, the Universe is again dominated by radiation.

To describe the evolution of this system, we have to use the Boltzmann equations that couple the time evolution of the ϕ energy density ρ_ϕ , the SM entropy density s , and the dark matter number density n_N [97–101],

³It redshifts as matter, $\rho_\phi \propto a^{-3}$.

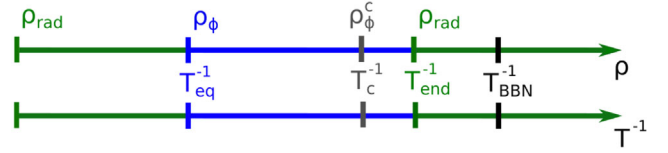


FIG. 3. Illustration of the density energy evolution and thermal history for a scalar matter field dominating in the early Universe. Here, the radiation-dominated dark matter freeze-out, discussed in Sec. III B, takes place in the green region (before T_{eq}^{-1}), while the matter-dominated freeze-out case, described in Sec. III C, happens in the blue region (after T_{eq}^{-1}) still before the energy density of the matter field takes a critical value ρ_ϕ^c at a critical temperature T_c .

$$\frac{d\rho_\phi}{dt} = -3H\rho_\phi - \Gamma_\phi \rho_\phi, \quad (36)$$

$$\frac{ds}{dt} = -3Hs + \frac{\Gamma_\phi \rho_\phi}{T} + 2\frac{E}{T} \langle \sigma v \rangle (n_N^2 - n_N^{\text{eq}2}), \quad (37)$$

$$\frac{dn_N}{dt} = -3Hn_N - \langle \sigma v \rangle (n_N^2 - n_N^{\text{eq}2}), \quad (38)$$

where $E \simeq m^2 + 3T^2$ is the averaged energy per dark matter particle.⁴ From Eqs. (37) and (38), one could see that the injected entropy into SM radiation produced by the decay of ϕ can dilute the thermally produced dark matter components. Actually, it happens for any freeze-out scenario before the end of ϕ decays [102].

In Fig. 3, we briefly recall the early thermal history prior to BBN. The ERD takes place up to the temperature T_{eq} at which the ρ_ϕ domination starts. Thereafter, ρ_ϕ effectively dominates over ρ_R at the temperature T_c , and the decay of ϕ ends at temperature T_{end} at which the radiation dominates back again.

The temperature T_{end} is one of the free parameters that specify the cosmological background. It is defined as [98,102]

$$T_{\text{end}} \equiv \left[\frac{90M_{\text{Pl}}^2}{\pi^2 g_\star(T_{\text{end}})} \right]^{1/4} \Gamma_\phi^{1/2}, \quad (39)$$

where Γ_ϕ stands for the total decay rate of ϕ into SM radiation. BBN restricts $T_{\text{end}} \gtrsim 4$ MeV [105–107]. The other free parameter is

$$\kappa = \left. \frac{\rho_\phi}{\rho_R} \right|_{T=m_N}, \quad (40)$$

⁴This set of equations does not consider the possibility of the ϕ decays also into dark matter particles because we assume ϕ does not decay into dark matter. That can be approximately realized, having this scalar field as a singlet with no $B - L$ charges. Anyway, a more general set of equations is provided in [98,102]. Moreover, ϕ decaying into dark matter is explored in [97,103,104].

which is the ratio between the energy densities of the scalar field and radiation at $T = m_N$. As we will be varying the dark matter mass, this ratio needs to be recomputed accordingly.

Both parameters T_{end} and κ are essentials to determine the dilution resulted from the ϕ decay. Notice that the Hubble rate is generally given by

$$H = \frac{1}{\sqrt{3}M_{\text{Pl}}}(\rho_\phi + \rho_R + \rho_N)^{1/2}, \quad (41)$$

with the dark matter freeze-out happening at temperature T_f during the ERD as usual.

As the dark matter freezes out at a temperature higher than T_{eq} , i.e., $T_{\text{eq}} \ll T_f$, the Hubble in Eq. (41) is reduced to Eq. (28), which in terms of the time variable x becomes [102]

$$H_R(x) \simeq \frac{\pi}{3} \sqrt{\frac{g_\star}{10}} \frac{m_N^2}{M_{\text{Pl}}} x^{-2}. \quad (42)$$

We emphasize that dark matter decouples much before the decay of ϕ . Hence, the SM entropy is conserved, $ds/dt = 0$, and Eq. (38) turns into

$$\frac{dY_N}{dx} = -\frac{s\langle\sigma v\rangle}{H_R x} (Y_N^2 - Y_N^{\text{eq}2}), \quad (43)$$

which yields

$$Y_N^{\text{std}} = \frac{15}{2\pi\sqrt{10g_\star}} \frac{x_f}{m_N M_{\text{Pl}} \langle\sigma v\rangle}, \quad (44)$$

the standard solution for the comoving dark matter number density long after the freeze-out and much before the ϕ decays. In this way, the freeze-out temperature depends neither on T_{end} nor on κ [102]. As the dark matter abundance is firstly computed in the standard freeze-out case, but will be changed due to ϕ decay (as showed in Fig. 4), this modification is set by the entropy injection episode that yields a dilution factor defined as

$$D \equiv \frac{s(T_2)}{s(T_1)} = \left(\frac{T_2}{T_1}\right)^3. \quad (45)$$

The dilution factor is simply the ratio between the SM entropy density at temperatures immediately after T_2 and before T_1 , the decay of the scalar field. We remind the reader that a similar reasoning is done in textbooks to obtain the temperature difference between photon and neutrinos after e^+e^- annihilations. Assuming the instantaneous decay approximation, the conservation of energy results to

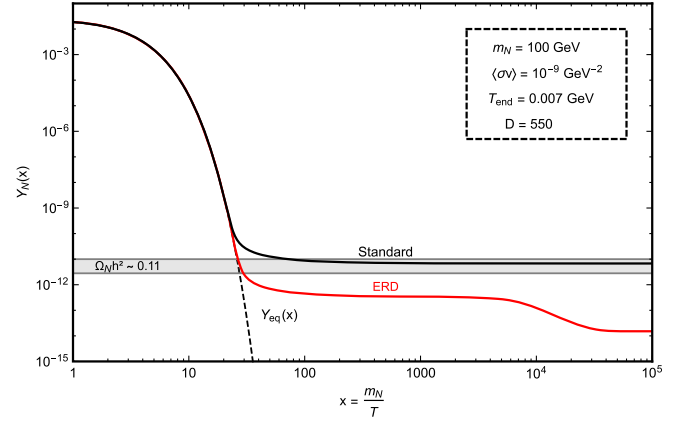


FIG. 4. Illustration of the yield *versus* x (red line) provided by a dark matter freeze-out happening during or before a matter-dominated period in the early Universe. For this case, we choose the dark matter mass $m_N = 100$ GeV and the annihilation cross section $\langle\sigma v\rangle = 10^{-9} \text{ GeV}^{-2}$. We choose $T_{\text{end}} = 0.007$ and $D = 550$. For completeness, we also include the yield for the standard case (black line). Again, the shaded gray region is the approximate range for the correct dark matter relic abundance as measured by Planck [13].

$$\rho_R(T_1) + \rho_\phi(T_1) = \rho_R(T_2). \quad (46)$$

As $\rho_\phi(m) = \kappa\rho_R(m)$, and taking $T_2 = T_{\text{end}}$, the dilution factor is

$$D = \kappa \frac{m_N}{T_{\text{end}}}. \quad (47)$$

In principle, D can take a wide range of values, but κ varies with the dark matter mass, and T_{end} should be larger than 4 MeV. Moreover, κ should be smaller than one at high temperatures to guarantee that the freeze-out happens during a radiation phase. Anyway, combining Eqs. (44) and (47), we obtain the final comoving dark matter number density [102],

$$Y_N = \frac{Y_N^{\text{std}}}{D}, \quad (48)$$

and consequently, the overall dark matter relic density is found,

$$\Omega_N h^2 = \frac{\Omega_N^{\text{std}} h^2}{D}, \quad (49)$$

where $\Omega_N^{\text{std}} h^2$ stands for the dark matter relic abundance computed in the standard radiation freeze-out scenario. Notice that one cannot randomly pick D at will, pick any dilution factor wished to salvage dark matter models from exclusions, because the value chosen for D is still connected to the dark matter mass and properties of the scalar field. Very large dilution factors are not feasible. Within this

production mechanism, we vary the free parameters ($g_X, m_N, m_Z, T_{\text{end}}, D$) to outline the region of parameter space consistent with existing bounds. In the next section, we obtain the dark matter relic density for freeze-out occurring while ρ_ϕ drives the expansion rate instead.

C. Freeze-out during early matter-dominated era

Pre-BBN thermal history is the same as discussed in the last section. Similarly, we consider an unstable scalar field ϕ in the early Universe which behaves as matter, $\omega_\phi = 0$. Moreover, before and after the ρ_ϕ dominates the expansion, the Universe is radiation-dominated. Now, we investigate the freeze-out process taking place during the period at which the scalar field ϕ governs the expansion rate. However, freeze-out happens much earlier than the decay of ϕ . Taking as reference Fig. 3, the freeze-out in this case happens between T_{eq}^{-1} and T_c^{-1} .

The Hubble parameter is found in Eq. (41). However, we define a temperature T_\star at which the ρ_ϕ begins to evolve. It allows us to parametrize the relative fraction of the total energy density at $T = T_\star$ in terms of [108],

$$r \equiv \frac{\rho_R + \rho_N}{\rho_\phi + \rho_R + \rho_N} \Big|_{T=T_\star} = \left[1 + \frac{g_\phi(T_\star)}{g_\star(T_\star) + g_N} \left(\frac{m_\phi}{T_\star} \right)^4 \right]^{-1}, \quad (50)$$

where $r \in [0, 1]$. In this way, for $T > T_\star > m_N$, we have

$$\frac{H^2}{H_\star^2} = \frac{g_\star r}{g_\star + g_N} \left(\frac{a_\star}{a} \right)^4 + (1-r) \left(\frac{a_\star}{a} \right)^3 + \frac{g_N r}{g_\star + g_N} \left(\frac{a_\star}{a} \right)^4, \quad (51)$$

where $H_\star \equiv H(T_\star)$ and $a_\star \equiv a(T_\star)$. The conservation of entropy leads to

$$\frac{a_\star}{a} \simeq \left(\frac{g_\star(T)}{g_\star(T_\star)} \right)^{1/4} \left(\frac{T}{T_\star} \right). \quad (52)$$

Inserting this result into Eq. (51), the Hubble parameter becomes, approximately,

$$H \simeq H_\star \left(\frac{g_\star(T)}{g_\star(T_\star)} \right)^{3/8} \left(\frac{T}{T_\star} \right)^{3/2} \left[(1-r) + r \left(\frac{T}{T_\star} \right) \right]^{1/2} \quad (53)$$

Thus, a matter domination phase arises immediately at T_\star [see Eq. (50)] for $r \ll 1$, which leads to $H \propto T^{3/2}$. For $r \simeq 1$, the Hubble rate goes as $H \propto T^2$, which is associated to a radiation-domination epoch. Anyway, the Universe is radiation-dominated at T_\star , and the matter domination phase will naturally arise at temperature

$$T_{\text{eq}} \equiv T_\star \left(\frac{a_\star}{a(T_{\text{eq}})} \right) = \frac{1-r}{r} \left[\frac{g_\star(T_\star)}{g_\star(T_{\text{eq}})} \right]^{1/4} T_\star, \quad (54)$$

at which ρ_ϕ accounts for 50% of the total density energy in agreement with [102,108].

The matter field that drives the expansion decays only when it effectively dominates over radiation at temperature

$$T_c \simeq (1-r)^{-1/3} \left[\frac{g_\star(T_{\text{end}}) T_{\text{end}}^4}{g_\star(T_\star) T_\star} \right]^{1/3}. \quad (55)$$

We stress that the freeze-out takes place in a matter domination period, which occurs much before the scalar field decays. In other words, the freeze-out temperature should lie in the range $T_c \ll T_f \ll T_{\text{eq}}$ [102,108].

We solve the Boltzmann equation for a matter-dominated universe, Eq. (38), with the Hubble given in Eq. (53). Taking the limiting case of matter domination, $r \ll 1$, and assuming an s -wave annihilation cross section, we find the comoving dark matter number density after freeze-out long after the matter domination epoch [108,109],

$$Y_N^{\text{MD}} = \frac{3}{2} \sqrt{\frac{45}{\pi}} \frac{\sqrt{g_\star} x_f^{3/2}}{g_{\star s} m_N M_{\text{Pl}} \langle \sigma v \rangle x_\star^{1/2}}, \quad (56)$$

where $x_\star = m_N/T_\star$ and $g_{\star s} \simeq g_\star \simeq cte$ at the time of freeze-out. However, it will be diluted due to entropy injection of the scalar field decay. In a similar vein, the dilution factor is the ratio between the entropy density computed at temperatures immediately before and after the scalar field decay, which in terms of T_{end} and T_\star leads to [109]⁵

$$\zeta = \frac{s(T_1)}{s(T_2)} \simeq (1-r)^{-1} \frac{g_\star(T_c) T_{\text{end}}}{g_\star(T_\star) T_\star}. \quad (57)$$

Therefore, the comoving dark matter number density becomes

$$Y_N = \zeta Y_N^{\text{MD}}, \quad (58)$$

and consequently,

$$\Omega_N h^2 = \zeta \Omega_N^{\text{MD}} h^2, \quad (59)$$

which is the dark matter relic density for a particle that freezes out during a matter domination era, which later experiences the decay of the scalar field ϕ . This scenario can also be represented by Fig. 4, where after freeze-out we see a dilution in the dark matter yield. In the next section, we present the constraints for our particle physics model.

⁵Notice that ζ may be equal to D^{-1} , but for a different freeze-out scenario and different parameters.

IV. CONSTRAINTS

As the model is based on a 2HDM fashion there are several constraints which have been derived specifically to the canonical 2HDM, but some are also applicable to our model with proper adjustments. We will cover them one-by-one below.

A. Collider

The most relevant collider limits stem from Z' searches at the LHC. As the Z' coupling to SM fermions is not suppressed, such a Z' boson can be easily produced at the LHC, giving rise to either dijet or dilepton signal events. If the Z' coupling to dark matter were different and larger than the one with SM fermions, the invisible decay of the Z' boson could be significant to weaken the LHC lower mass bound. However, in our model, the Z' field interacts with equal strength to all fermions. Thus, the dilepton and dijet searches at the LHC are not meaningfully impacted by the presence of Z' decays into dark matter pairs [110,111]. These two datasets have been considered, and the respective bounds are displayed in our plots.

B. Flavor physics

Interestingly, our model can also be constrained by flavor physics observed despite the absence of flavor changing interactions. The charged Higgs boson contributes to the $b \rightarrow s\gamma$ at the one-loop level via the Cabibbo–Kobayashi–Maskawa (CKM) matrix [112,113]. The limit is reported in terms of $\tan\beta$ and the charged scalar mass. In our model, the mass of the charged Higgs boson is proportional to the v_s , VEV of the singlet scalar, and $\tan\beta$. Taking $\tan\beta = 1$, we can convert the lower mass limit on the charged Higgs mass into a bound on v_s . Knowing that the Z' mass is controlled by v_s and g_X , for a given value of g_X we now have a constraint on the Z' mass. We exhibit this limit in our plots.

C. Atomic parity violation

Atomic parity violation (APV) effects are often overlooked in physics beyond the Standard Model endeavors [56,57,114,115]. The Z' gauge boson rising from the $B - L$ gauge group has only vectorial interactions with fermions. In principle, that would lead to no APV, but in the presence of mass mixing with the Z boson this is no longer true. Atomic transitions in Cesium has proven to be a great laboratory to probe Z' contributions to APV via mass mixing. Following [74], the contribution to the weak charge of Cesium in our model is found to be

$$\Delta Q_W = -59.84\delta^2 - 220\delta \sin\theta_W \cos\theta_W e \frac{m_Z}{m_{Z'}} - 133\delta^2 \tan\beta^2, \quad (60)$$

where δ is the mass mixing parameter

$$\delta = \frac{\cos\beta \cos\beta_d}{\sqrt{1 - \cos^2\beta \cos^2\beta_d}}, \quad (61)$$

and where we have defined $\tan\beta_d = \frac{v_1}{v_s}$ [49]. As the v_s controls the Z' mass, with $\tan\beta = 1$, we can display this limit in terms of the Z' mass for a given g_X . We show this constraint in our plots.

D. Direct detection

Dark matter particles might scatter off of nuclei, leaving a signal at direct detection experiments. We are considering heavy mediators only, thus the momentum transfer in the scattering process is much smaller than the mediator mass. Therefore, the dark matter interaction with quarks can be treated using effective operators. Our model features the effective Lagrangian

$$\mathcal{L}_{DD} = \frac{g_X^4}{18m_{Z'}^2} \bar{N}_{1R} \gamma^\mu \gamma_5 N_{1R} \bar{q} \gamma_\mu q, \quad (62)$$

where $q = u, d$. We point out that only the valence quarks contribute due to the vector current present in Eq. (62).

In models where $Z - Z'$ mass mixing is absent, Eq. (62) represents the only relevant source of the direct detection signal. Interestingly, such a term does not give rise to the standard spin-independent (SI) or spin-dependent (SD) dark-matter-nucleon scattering signal. Hence, we need to map this Lagrangian onto a more general formalism using effective operators [116–118] to understand that this interaction gives rise to the operators

$$\bar{N}_{1R} \gamma^\mu \gamma_5 N_{1R} \bar{q} \gamma_\mu q \rightarrow 2\vec{v}_N^\perp \cdot \vec{S}_N + 2i\vec{S}_N \cdot \left(\vec{S}_n \times \frac{\vec{q}}{m_N} \right), \quad (63)$$

where $\vec{S}_N = 1/2$ is the right-handed neutrino spin, \vec{S}_n the net nucleus spin, $\vec{v}_N^\perp = \vec{v} + \frac{\vec{q}}{2\mu}$, \vec{q} is the momentum transfer, and μ the reduced mass.

The first term in Eq. (63) features an enhancement with the atomic mass but is velocity suppressed, whereas the second is momentum suppressed and spin-dependent. That said, the first term will be dominant but will yield a distinct energy spectrum at the detector. We properly account for this behavior using the code described in [119].

However, our model has a second Higgs doublet charged under the new gauge symmetry. Therefore, the $Z - Z'$ mass mixing is unavoidable. This mixing induces the operator,

$$\mathcal{L}_{DD} = \frac{1}{\Lambda^2} \bar{N}_{1R} \gamma^\mu \gamma_5 N_{1R} \bar{q} \gamma_\mu \gamma^5 q, \quad (64)$$

where Λ here encodes both the Z mediator and the Z' mediator via t-channel diagrams. This axial-vector interaction is known to generate a spin-dependent scattering, which is found to be

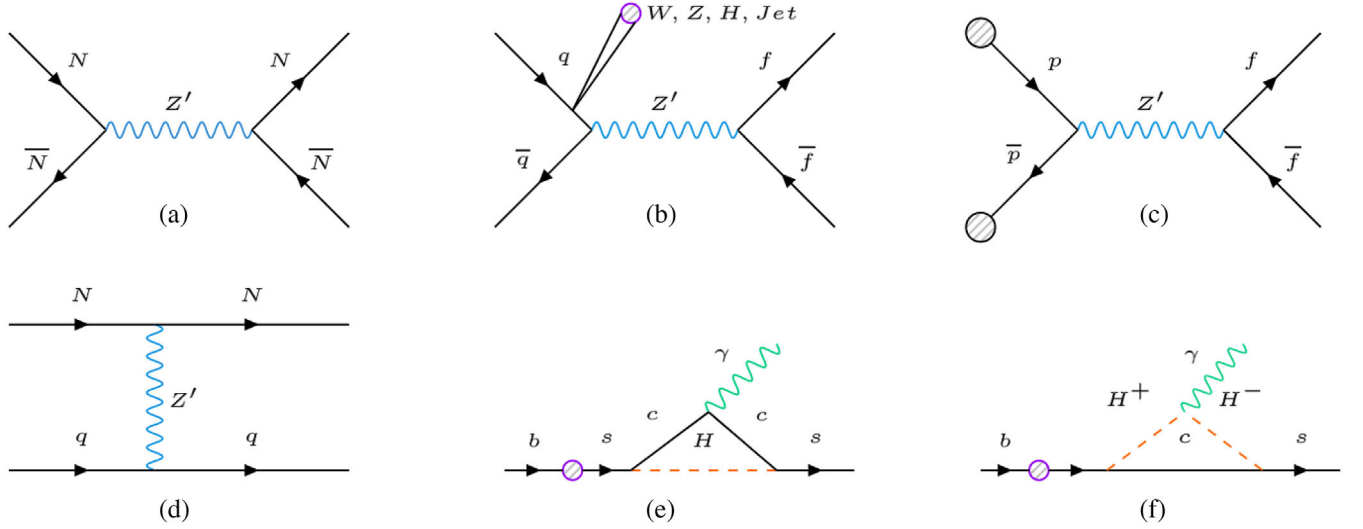


FIG. 5. Here we have the Feynman diagrams related to the dark matter phenomenology of this work. The diagram (a) gives the dark matter relic abundance, (b) corresponds to collider searches, (c) is associated with the atomic parity violation bounds, (d) to direct detection searches, and (e) & (f) come from flavor physics.

$$\sigma_{\text{Np}}^{\text{SD}} = \frac{\mu_{\text{Np}}^2}{4\pi} \left| \left(\frac{g_{Z'u}^A g_{ZN}}{m_Z^2} + \frac{g_{Z'u}^A g_{Z'N}}{m_{Z'}^2} \right) \Delta_u^p + \left(\frac{g_{Z'd}^A g_{ZN}}{m_Z^2} + \frac{g_{Z'd}^A g_{Z'N}}{m_{Z'}^2} \right) (\Delta_d^p + \Delta_s^p) \right|^2, \quad (65)$$

where $g_{Z'u,d}^A$ ($g_{Z'u,d}^A$) are the axial couplings of the Z (Z') boson with quarks, while g_{ZN} ($g_{Z'N}$) are the axial couplings of the Z (Z') boson with dark matter. The explicit expressions can be extracted directly from Eq. (16), and $\Delta_{u,d,s}^p$ are form factors accounting for the light quark contributions to the nucleon spin [116,117].

V. RESULTS

In this section, we present the results for each scenario described above. We compute the dark matter relic density for different cosmological setups and compare the aforementioned bounds. The results are presented in the $m_{Z'}$ vs m_N plane. We cover several cosmological scenarios, varying their cosmological parameters. We also fixed the gauge coupling, $g_X = 1$, since the main focus here is to study the impact of different cosmological parameters on this model. In any case, decreasing the gauge coupling g_X will provide lower cross sections, leading to higher relic densities. To compensate for this change and to get the right relic density, we have to diminish the Z' mass, usually leading to more constrained scenarios.⁶ For completeness, we also include the main Feynman diagrams responsible for the dark matter relic density, collider and direct searches, atomic parity violation, and flavor physics in Fig. 5.

⁶For a detailed study on the impact of the gauge coupling on the results, we recommend [74].

We assess the impact of nonstandard cosmology by comparing our findings with those stemming from a standard freeze-out. The colorful shaded regions represent the bounds from direct detection (blue region), dijet (red region), dilepton (cyan region), flavor physics (light green), APV (dark green region), and perturbative unitarity (magenta). We overlay the curves that delimit the parameter, yielding the correct relic density within the standard freeze-out (solid black).

A. Faster than usual early expansion

In the standard freeze-out case, the right-handed neutrino dark matter can nicely reproduce the correct relic density and evade existing bounds around the Z' resonance, and away from the resonance when $m_N > m_{Z'}$. In the context of a faster expansion rate at early times, the (n, T_r) parameters have an enormous impact on the dark matter relic abundance [87,120]. Moreover, the dark matter mass also plays a key role. We explore $n = 2, 4, 6$ cosmologies, for temperatures $T_r = 0.1, 1, 10$ GeV, to have an overall idea of how a faster expansion affects the standard relic density. The largest temperature at the end of the relentless phase should be $T_r = 10$ GeV, because we must enforce $T_f > T_r$ to keep freeze-out occurring during the scalar field domination. That said, we exhibit in Fig. 6 the region of the parameter in the m_N vs $m_{Z'}$ plane that yields the correct relic density. For comparison, we also display with a black curve the region of parameter space that gives the right relic density in the standard freeze-out regime. For all plots we took $g_X = 1$, in the top-left panel we adopted $n = 2$, in the top-right panel we assumed $n = 4$, and in the bottom plot $n = 6$.

It is clear that the parameters n and T_r can enhance the dark matter relic density. We explored an interplay

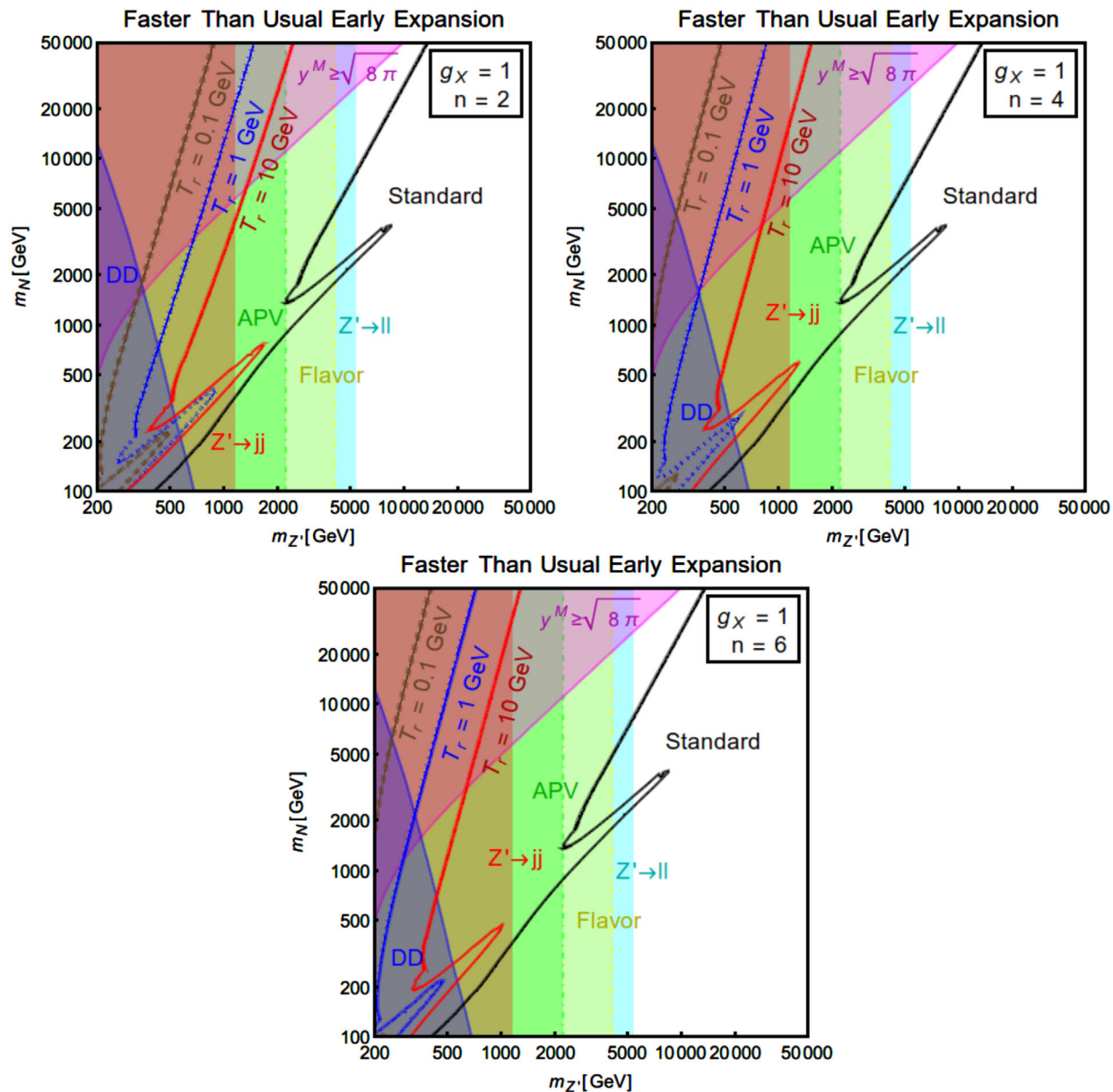


FIG. 6. Fast expansion case: We exhibit the curves that delimit the parameter space that leads to the correct relic density for $T_r = 0.1$ (brown), 1 GeV (blue), and 10 GeV (red). We also display the region which reproduces the correct relic density within the standard freeze-out for comparison. The colorful shaded regions represent the bounds from direct detection (blue region), dijet (red region), dilepton (cyan region), flavor physics (light green), APV (dark green region), and perturbative unitarity (magenta).

between n and T_r , keeping one fixed and varying the other. Due to the enhancement of the dark matter abundance from a faster, with respect to standard cosmology, expansion rate of the Universe, a viable relic density requires lower values of the mass of the Z' to be achieved. One can understand this conclusion, remembering that the Z' mass enters the denominator of the thermal annihilation cross section. Hence, the smaller the Z' mass, the smaller the abundance. This shift to lower Z' masses appears to counterbalance the fast expansion present during the dark matter freeze-out. As we increase further the expansion rate and take $n = 4$ (top-right

panel), and $n = 6$ (bottom panel), the regions that reproduce the correct relic are also further shifted to smaller Z' masses. Furthermore, for each cosmological background n , the larger the ratio $x_r = m_N/T_r$, the longer the relentless phase. Then, for a fixed T_r , the heavier the right-handed neutrino dark matter particles, the larger the Z' masses (smaller cross sections) to compensate for the suppression of the dark matter relic density due to their longer time relentlessly annihilating.

The slope of the curves is mostly governed by n as it is closely related to the equation of state of the field ϕ [87]. Notice that this fast expansion history is completely

excluded by existing bounds, even in the Z' resonance. In the face of this, we will explore the impact of the early matter-dominated field on this model.

B. Matter field domination in the early Universe

In this section, we deal with the nonstandard freeze-out scenarios discussed in Secs. III B and III C. Here, we use the cosmological parameters (T_{end}, D) and (T_*, ζ) for ERD and EMD, respectively. We firstly analyze the early radiation-dominated freeze-out, thereafter, the dark matter decoupling during EMD in which the field ϕ drives the Hubble expansion, but is still away from its decay.

1. Freeze-out during early radiation-dominated era followed by a matter domination period

In this case, we explore $D = 550$ and 2750 , fixing $T_{\text{end}} = 0.007$ GeV [98]. As discussed earlier, κ is not fixed in order to adjust to the dark matter mass scales [see Eq. (47)]. It is common to evoke a constant and *ad hoc* dilution factor to bring down the dark matter relic density and circumvent existing bounds. Notice that this dilution factor cannot take any value, because it does depend on T_{end} and κ . Naively, one might think that κ and T_{end} are completely independent parameters. As κ is the ratio between the ϕ and radiation densities, thus it depends on $g_*(T_{\text{end}})/g_*(T = m_N)$ [102]. Therefore, κ does feature a dependence on T_{end} . As we need to impose $T_{\text{end}} > 4$ MeV due to BBN bounds, clearly the dilution factor D cannot take arbitrarily large values.

In Fig. 7, we see that the contours that delimit the region of parameter space which yield the right dark matter abundance are free from existing bounds even away from the resonance, for $m_N < m_{Z'}$. Notice that the larger the entropy after the decay of the scalar field quantified by the dilution factors $D = 550$ and 2750 , the smaller the cross sections and the lighter the dark matter masses that are required to obtain the correct relic density. In other words, there is a shift towards heavier Z' bosons and smaller dark matter masses. It is important to emphasize that we are fixing the value of $T_{\text{end}} = 0.007$ and leaving the κ parameter free to get the right value of the dilution factor. If we fix the mass m and the κ parameter, T_{end} will be inversely proportional to the dilution factor D , according to Eq. (47). Conversely, the region of parameter space that reproduces the correct relic density in the standard freeze-out is rather more constrained. Hence, a successful way to salvage WIMP models from restrictive direct detection and collider bounds is to assume a standard freeze-out followed by a short matter domination stage governed by the scalar ϕ , which then decays and injects entropy, shifting the relic density curve to the right side in Fig. 7.

2. Freeze-out during early matter-dominated era

In Fig. 8, we show the results for the early matter-dominated freeze-out. We have chosen $\zeta = 10^{-6}$ and

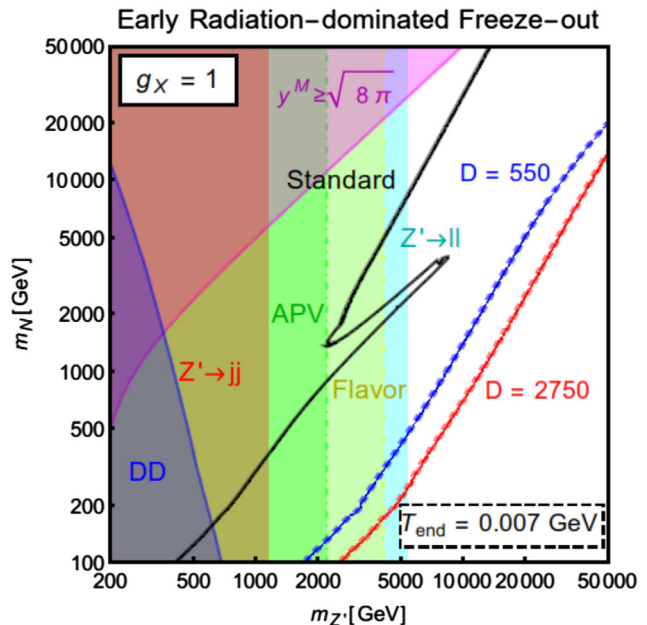


FIG. 7. The correct dark matter relic abundance for dark matter freeze-out happening during the early radiation-dominated epoch. For $g_X = 1$, the cosmological parameters are fixed to $T_{\text{end}} = 0.007$ GeV and $D = 550$ and 2750 (blue and red curves, respectively). The constraints are the same as in Fig. 6.

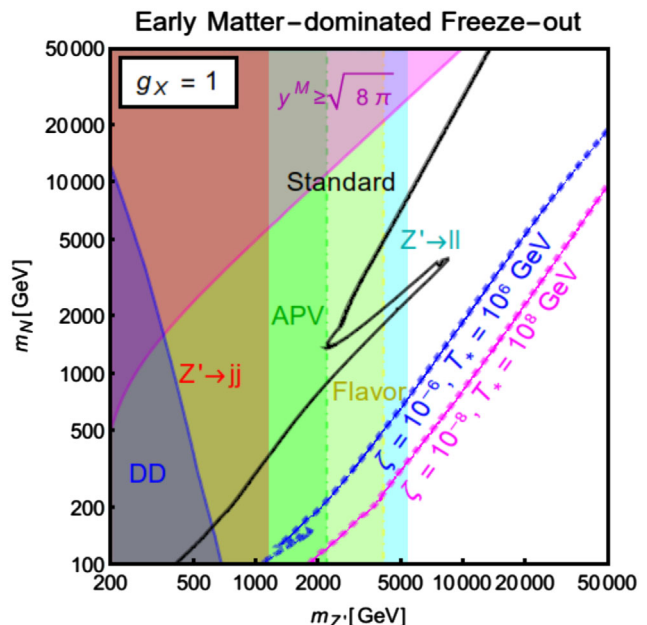


FIG. 8. The correct dark matter relic abundance for dark matter freeze-out happening during the matter-dominated epoch before the decay of ϕ . For $g_X = 1$, the cosmological parameters are set into pairs of ζ and T_* . We have chosen $\zeta = 10^{-6}$ and $T_* = 10^6$ GeV (blue curve), and $\zeta = 10^{-8}$ and $T_* = 10^8$ GeV (magenta curve). The constraints are the same as in Fig. 6.

$T_\star = 10^6$ GeV, and $\zeta = 10^{-8}$ and $T_\star = 10^8$ GeV. These choices are in agreement with the freeze-out during the EMD condition, namely, $T_c \ll T_f \ll T_{\text{eq}}$. We took $T_{\text{end}} \simeq 10$ GeV, and $r = 0.99$. The blue and magenta curves delimit the region of parameter space that yields the correct relic density. It is visible that most regions of parameter space are now consistent with existing bounds.

Our results comparing the standard case (black lines) lead to scenarios completely free from the bounds for dark matter masses larger than 200 GeV, for both ERD and EMD cases. On the other side, for the standard case, the only regions that survive the limits are near the Z' resonance. Therefore, for our model, the search for dark matter masses around the TeV scale may hint at the presence of non-standard cosmological histories in the early Universe.

C. The relentless phase *versus* the entropy injection

In this section, we put all results into perspective and discuss the key findings concerning the overall dark matter density in the presence of nonstandard cosmologies. In Fig. 9, we present the results for the scenarios in which a quintessence fluid (red curve) with $n = 2$ and $T_r = 10$ GeV dominates the expansion rate (faster expansion), the standard ERD (but is followed by the decay of a matter field for $D = 550$ with $T_{\text{end}} = 0.007$ GeV) and lastly the freeze-out occurs during EMD for $\zeta = 10^{-8}$ and $T_\star = 10^8$ GeV.

It is remarkable that for a quintessence-dominated freeze-out, the contour arises in the left-hand side of the

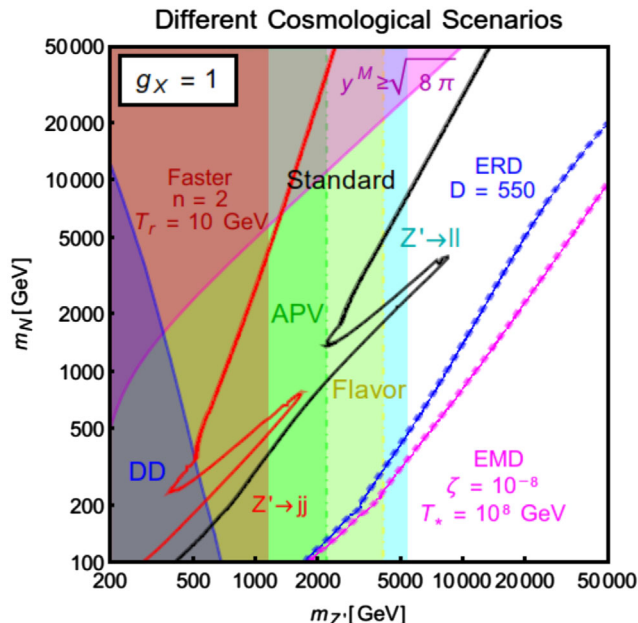


FIG. 9. The correct dark matter relic abundance is presented for the *quintessence* fluid $n = 2$ (solid red contour), the early radiation-dominated freeze-out case (blue contour), and for the freeze-out during the EMD (magenta contour). We took $T_r = 10$ GeV, $D = 550$, and $\zeta = 10^{-8}$ and $T_\star = 10^8$ GeV, respectively. The constraints are still the same as in Fig. 6.

standard freeze-out. This reflects the fact that the larger the Hubble rate, the larger the annihilation cross section to reproduce the correct relic density.

Instead, for freeze-out happening during periods in which the Hubble rate is equivalent to or slower than radiation, the contour appears in the right-hand side, which is less constrained by data. Hence, the presence of a scalar field that drives the Hubble rate during or after the dark matter freeze-out represents an important direction to be explored by the next generation of experiments.

VI. CONCLUSIONS

In this work, we investigated the dark matter phenomenology of a weak-scale right-handed neutrino dark matter under three different cosmological settings. We concretely incorporated this right-handed neutrino into a two Higgs doublet model featuring an Abelian gauge symmetry. The model itself is well motivated for being able to account for neutrino masses and the absence of flavor changing interactions in the scalar sector.

The dark matter phenomenology is driven by the presence of a Z' field, as well as by the $Z - Z'$ mass mixing that arises because a Higgs doublet is involved in the spontaneous symmetry breaking of the new Abelian gauge symmetry. Concerning nonstandard cosmology, we explored the case where the universe expands faster than usual, and the scenarios where the dark matter freeze-out takes place during a matter domination epoch, as well as during a usual radiation domination, but it is then followed by a matter domination phase.

For the faster expanding case, we found a very constrained scenario, since larger cross sections are necessary to reproduce the right relic density, whereas when a matter field dominates the expansion rate in the early Universe either during or after the dark matter freeze-out the relic density curves are shifted away from existing bounds. After putting our results into perspective with flavor bounds, direct detection, colliders and atomic parity violation, we solidly conclude that the weak-scale right-handed neutrino stands for a plausible dark matter candidate in the presence of an early matter domination epoch.

ACKNOWLEDGMENTS

F. S. Q. and C. S. have been supported by the São Paulo Research Foundation (FAPESP) through Grant No. 2015/15897-1. C. S. is supported by Grant No. 2020/00320-9, São Paulo Research Foundation (FAPESP). F. S. Q. acknowledges support from CNPq Grants No. 303817/2018-6 and No. 421952/2018-0, and ICTP-SAI FR FAPESP Grant No. 2016/01343-7, MEC, and UFRN. This work was supported by the Serrapilheira Institute (Grant No. Serra-1912-31613) and ANID Millennium Program ICN2019044. The author J. P. N. acknowledges the support from CAPES under the Grant No. 88887.484542/2020-00.

- [1] N. Aghanim *et al.* (Planck Collaboration), Planck 2018 results. VI. Cosmological parameters, *Astron. Astrophys.* **641**, A6 (2020).
- [2] G. Arcadi, M. Dutra, P. Ghosh, M. Lindner, Y. Mambrini, M. Pierre, S. Profumo, and F. S. Queiroz, The waning of the WIMP? A review of models, searches, and constraints, *Eur. Phys. J. C* **78**, 203 (2018).
- [3] R. K. Leane, T. R. Slatyer, J. F. Beacom, and K. C. Y. Ng, GeV-scale thermal WIMPs: Not even slightly ruled out, *Phys. Rev. D* **98**, 023016 (2018).
- [4] S. Fukuda *et al.* (Super-Kamiokande Collaboration), Constraints on Neutrino Oscillations using 1258 Days of Super-Kamiokande Solar Neutrino Data, *Phys. Rev. Lett.* **86**, 5656 (2001).
- [5] Q. R. Ahmad *et al.* (SNO Collaboration), Direct Evidence for Neutrino Flavor Transformation from Neutral Current Interactions in the Sudbury Neutrino Observatory, *Phys. Rev. Lett.* **89**, 011301 (2002).
- [6] S. Abe *et al.* (KamLAND Collaboration), Precision Measurement of Neutrino Oscillation Parameters with KamLAND, *Phys. Rev. Lett.* **100**, 221803 (2008).
- [7] K. Abe *et al.* (T2K Collaboration), Indication of Electron Neutrino Appearance from an Accelerator-produced Off-axis Muon Neutrino Beam, *Phys. Rev. Lett.* **107**, 041801 (2011).
- [8] Y. Abe *et al.* (Double Chooz Collaboration), Indication of Reactor $\bar{\nu}_e$ Disappearance in the Double Chooz Experiment, *Phys. Rev. Lett.* **108**, 131801 (2012).
- [9] F. P. An *et al.* (Daya Bay Collaboration), Observation of Electron-Antineutrino Disappearance at Daya Bay, *Phys. Rev. Lett.* **108**, 171803 (2012).
- [10] J. K. Ahn *et al.* (RENO Collaboration), Observation of Reactor Electron Antineutrino Disappearance in the RENO Experiment, *Phys. Rev. Lett.* **108**, 191802 (2012).
- [11] P. Adamson *et al.* (MINOS Collaboration), Electron Neutrino and Antineutrino Appearance in the Full MINOS Data Sample, *Phys. Rev. Lett.* **110**, 171801 (2013).
- [12] K. N. Abazajian *et al.*, Neutrino physics from the cosmic microwave background and large scale structure, *Astropart. Phys.* **63**, 66 (2015).
- [13] N. Aghanim, Y. Akrami, M. Ashdown, J. Aumont, C. Baccigalupi, M. Ballardini, A. J. Banday, R. B. Barreiro, N. Bartolo *et al.*, Planck 2018 results, *Astron. Astrophys.* **641**, A6 (2020).
- [14] M. Aoki, S. Kanemura, and O. Seto, Neutrino mass, Dark Matter and Baryon Asymmetry via TeV-Scale Physics without Fine-Tuning, *Phys. Rev. Lett.* **102**, 051805 (2009).
- [15] T. Nomura and H. Okada, Hidden $U(1)$ gauge symmetry realizing a neutrinophilic Two-Higgs-Doublet model with dark matter, *Phys. Rev. D* **97**, 075038 (2018).
- [16] T. Nomura and H. Okada, Neutrinophilic Two Higgs Doublet model with dark matter under an alternative $U(1)_{B-L}$ gauge symmetry, *Eur. Phys. J. C* **78**, 189 (2018).
- [17] H. Cai, T. Nomura, and H. Okada, A neutrino mass model with hidden $U(1)$ gauge symmetry, *Nucl. Phys.* **B949**, 114802 (2019).
- [18] J. Gehrlein and M. Pierre, A testable hidden-sector model for Dark Matter and neutrino masses, *J. High Energy Phys.* **02** (2020) 068.
- [19] D. Van Loi, P. Van Dong, and D. Van Soa, Neutrino mass and dark matter from an approximate $B-L$ symmetry, *J. High Energy Phys.* **05** (2020) 090.
- [20] S. Singirala, R. Mohanta, S. Patra, and S. Rao, Majorana dark matter, massless goldstone and neutrino mass in a new $B-L$ model, *Springer Proc. Phys.* **234**, 315 (2019).
- [21] P. Di Bari, Neutrino masses, leptogenesis and dark matter, [arXiv:1904.11971](https://arxiv.org/abs/1904.11971).
- [22] S. Mishra, S. Singirala, and S. Sahoo, Scalar dark matter, neutrino mass and leptogenesis in a $U(1)$ model, *J. Phys. G* **48**, 075003 (2021).
- [23] W. Chao, M. Gonderinger, and M. J. Ramsey-Musolf, Higgs vacuum stability, neutrino mass, and dark matter, *Phys. Rev. D* **86**, 113017 (2012).
- [24] D. Restrepo, A. Rivera, and W. Tangarife, Singlet-doublet dirac dark matter and neutrino masses, *Phys. Rev. D* **100**, 035029 (2019).
- [25] A. Das, S. Goswami, K. N. Vishnudath, and T. Nomura, Constraining a general $U(1)$ inverse seesaw model from vacuum stability, dark matter and collider, *Phys. Rev. D* **101**, 055026 (2020).
- [26] C. Jaramillo, M. Lindner, and W. Rodejohann, Seesaw neutrino dark matter by freeze-out, *J. Cosmol. Astropart. Phys.* **04** (2021) 023.
- [27] J. A. Dror, D. Dunsky, L. J. Hall, and K. Harigaya, Sterile neutrino dark matter in left-right theories, *J. High Energy Phys.* **07** (2020) 168.
- [28] P. Van Dong, Flipping principle for neutrino mass and dark matter, *Phys. Rev. D* **102**, 011701 (2020).
- [29] S. Dodelson and L. M. Widrow, Sterile-Neutrinos as Dark Matter, *Phys. Rev. Lett.* **72**, 17 (1994).
- [30] T. Asaka, S. Blanchet, and M. Shaposhnikov, The nuMSM, dark matter and neutrino masses, *Phys. Lett. B* **631**, 151 (2005).
- [31] V. De Romeri, D. Karamitros, O. Lebedev, and T. Toma, Neutrino dark matter and the higgs portal: improved freeze-in analysis, *J. High Energy Phys.* **10** (2020) 137.
- [32] A. D. Dolgov and S. H. Hansen, Massive sterile neutrinos as warm dark matter, *Astropart. Phys.* **16**, 339 (2002).
- [33] K. Abazajian, G. M. Fuller, and M. Patel, Sterile neutrino hot, warm, and cold dark matter, *Phys. Rev. D* **64**, 023501 (2001).
- [34] K. Abazajian, Production and evolution of perturbations of sterile neutrino dark matter, *Phys. Rev. D* **73**, 063506 (2006).
- [35] T. Asaka, M. Laine, and M. Shaposhnikov, Lightest sterile neutrino abundance within the nuMSM, *J. High Energy Phys.* **01** (2007) 091. Erratum, *J. High Energy Phys.* **02** (2015) 028.
- [36] A. Kusenko, Sterile neutrinos: The dark side of the light fermions, *Phys. Rept.* **481**, 1 (2009).
- [37] F. S. Queiroz and K. Sinha, The poker face of the majoron dark matter model: LUX to keV line, *Phys. Lett. B* **735**, 69 (2014).
- [38] C. Garcia-Cely and J. Heeck, Neutrino lines from majoron dark matter, *J. High Energy Phys.* **05** (2017) 102.
- [39] K. N. Abazajian, Sterile neutrinos in cosmology, *Phys. Rep.* **711–712**, 1 (2017).
- [40] A. Boyarsky, M. Drewes, T. Lasserre, S. Mertens, and O. Ruchayskiy, Sterile neutrino dark matter, *Prog. Part. Nucl. Phys.* **104**, 1 (2019).

- [41] X.-D. Shi and G. M. Fuller, A New Dark Matter Candidate: Nonthermal Sterile Neutrinos, *Phys. Rev. Lett.* **82**, 2832 (1999).
- [42] A. Schneider, Astrophysical constraints on resonantly produced sterile neutrino dark matter, *J. Cosmol. Astropart. Phys.* **04** (2016) 059.
- [43] M. Ahmadvand, Matter and dark matter asymmetry from a composite higgs model, *Eur. Phys. J. C* **81**, 358 (2021).
- [44] M. Ahmadvand, Filtered asymmetric dark matter during the Peccei-Quinn phase transition, *J. High Energy Phys.* **10** (2021) 109.
- [45] N. Okada and O. Seto, Higgs portal dark matter in the minimal gauged $U(1)_{B-L}$ model, *Phys. Rev. D* **82**, 023507 (2010).
- [46] N. Okada and S. Okada, Z' -portal right-handed neutrino dark matter in the minimal $U(1)_X$ extended Standard Model, *Phys. Rev. D* **95**, 035025 (2017).
- [47] N. Okada and S. Okada, Z'_{BL} portal dark matter and LHC Run-2 results, *Phys. Rev. D* **93**, 075003 (2016).
- [48] S. Okada, Z' portal dark matter in the minimal $B-L$ Model, *Adv. High Energy Phys.* **2018**, 5340935 (2018).
- [49] M. D. Campos, D. Cogollo, M. Lindner, T. Melo, F. S. Queiroz, and W. Rodejohann, Neutrino masses and absence of flavor changing interactions in the 2HDM from gauge principles, *J. High Energy Phys.* **08** (2017) 092.
- [50] D. A. Camargo, L. Delle Rose, S. Moretti, and F. S. Queiroz, Collider bounds on 2-Higgs doublet models with $U(1)_X$ gauge symmetries, *Phys. Lett. B* **793**, 150 (2019).
- [51] S. Blasi, V. Brdar, and K. Schmitz, Fingerprint of low-scale leptogenesis in the primordial gravitational-wave spectrum, *Phys. Rev. Research* **2**, 043321 (2020).
- [52] W.-C. Huang, H. Ishida, C.-T. Lu, Y.-L. S. Tsai, and T.-C. Yuan, Signals of new gauge bosons in gauged Two Higgs Doublet model, *Eur. Phys. J. C* **78**, 613 (2018).
- [53] E. Accomando, L. Delle Rose, S. Moretti, E. Olaiya, and C. H. Shepherd-Themistocleous, Extra Higgs boson and Z' as portals to signatures of heavy neutrinos at the LHC, *J. High Energy Phys.* **02** (2018) 109.
- [54] A. Arhrib, W.-C. Huang, R. Ramos, Y.-L. S. Tsai, and T.-C. Yuan, Consistency of a gauged Two-Higgs-Doublet model: Scalar sector, *Phys. Rev. D* **98**, 095006 (2018).
- [55] C.-T. Huang, R. Ramos, V. Q. Tran, Y.-L. S. Tsai, and T.-C. Yuan, Consistency of gauged Two Higgs Doublet model: Gauge sector, *J. High Energy Phys.* **09** (2019) 048.
- [56] H. Davoudiasl, H.-S. Lee, and W. J. Marciano, 'Dark' Z implications for parity violation, rare meson decays, and Higgs physics, *Phys. Rev. D* **85**, 115019 (2012).
- [57] H. Davoudiasl, H.-S. Lee, and W. J. Marciano, Muon Anomaly and Dark Parity Violation, *Phys. Rev. Lett.* **109**, 031802 (2012).
- [58] M. Lindner, F. S. Queiroz, W. Rodejohann, and X.-J. Xu, Neutrino-electron scattering: General constraints on Z' and dark photon models, *J. High Energy Phys.* **05** (2018) 098.
- [59] A. G. Dias, J. Leite, and D. S. V. Gonçalves, Axion-neutrino interplay in a gauged Two-Higgs-Doublet model, *Phys. Rev. D* **104**, 075014 (2021).
- [60] P. Ko, Y. Omura, and C. Yu, Higgs phenomenology in Type-I 2HDM with $U(1)_H$ Higgs gauge symmetry, *J. High Energy Phys.* **01** (2014) 016.
- [61] C.-R. Chen, Y.-X. Lin, V. Q. Tran, and T.-C. Yuan, Pair production of Higgs bosons at the LHC in gauged 2HDM, *Phys. Rev. D* **99**, 075027 (2019).
- [62] D. A. Camargo, M. Klasen, and S. Zeinstra, Discovering heavy $U(1)$ -gauged Higgs bosons at the HL-LHC, *J. Phys. G* **48**, 025002 (2020).
- [63] J. Heeck and W. Rodejohann, Gauged $L_\mu - L_\tau$ symmetry at the electroweak scale, *Phys. Rev. D* **84**, 075007 (2011).
- [64] D. A. Camargo, A. G. Dias, T. B. de Melo, and F. S. Queiroz, Neutrino masses in a Two Higgs Doublet model with a $U(1)$ gauge symmetry, *J. High Energy Phys.* **04** (2019) 129.
- [65] D. Cogollo, R. D. Matheus, T. B. de Melo, and F. S. Queiroz, Type I + II seesaw in a Two Higgs Doublet model, *Phys. Lett. B* **797**, 134813 (2019).
- [66] M. Lindner, M. Platscher, and F. S. Queiroz, A call for new physics: The muon anomalous magnetic moment and lepton flavor violation, *Phys. Rep.* **731**, 1 (2018).
- [67] F. J. Botella, F. Cornet-Gomez, and M. Nebot, Flavor conservation in Two-Higgs-Doublet models, *Phys. Rev. D* **98**, 035046 (2018).
- [68] A. Ordell, R. Pasechnik, H. Serôdio, and F. Nottensteiner, Classification of anomaly-free 2HDMs with a gauged $U(1)'$ symmetry, *Phys. Rev. D* **100**, 115038 (2019).
- [69] P. M. Ferreira, B. Grzadkowski, O. M. Ogreid, and P. Osland, Symmetries of the 2HDM: An invariant formulation and consequences, *J. High Energy Phys.* **02** (2021) 196.
- [70] P. Ko, Y. Omura, and C. Yu, Dark matter and dark force in the type-I inert 2HDM with local $U(1)_H$ gauge symmetry, *J. High Energy Phys.* **11** (2014) 054.
- [71] D. A. Camargo, M. D. Campos, T. B. de Melo, and F. S. Queiroz, A two Higgs doublet model for dark matter and neutrino masses, *Phys. Lett. B* **795**, 319 (2019).
- [72] C.-R. Chen, Y.-X. Lin, C. S. Nugroho, R. Ramos, Y.-L. S. Tsai, and T.-C. Yuan, Complex scalar dark matter in the gauged Two-Higgs-Doublet model, *Phys. Rev. D* **101**, 035037 (2020).
- [73] M. Lindner, Y. Mambrini, T. B. de Melo, and F. S. Queiroz, XENON1T anomaly: A light Z' from a Two Higgs Doublet model, *Phys. Lett. B* **811**, 135972 (2020).
- [74] G. Arcadi, S. Profumo, F. S. Queiroz, and C. Siqueira, Right-handed neutrino dark matter, neutrino masses, and non-standard cosmology in a 2HDM, *J. Cosmol. Astropart. Phys.* **12** (2020) 030.
- [75] B. Dirgantara and C. S. Nugroho, Effects of new heavy fermions on complex scalar dark matter phenomenology in gauged Two Higgs Doublet model, *arXiv:2012.13170*.
- [76] L. Delle Rose, S. Khalil, and S. Moretti, Explanation of the 17 MeV Atomki anomaly in a $U(1)'$ -extended Two Higgs Doublet model, *Phys. Rev. D* **96**, 115024 (2017).
- [77] L. Delle Rose, S. Khalil, S. J. D. King, S. Moretti, and A. M. Thabt, Atomki anomaly in family-dependent $U(1)$ extension of the Standard Model, *Phys. Rev. D* **99**, 055022 (2019).
- [78] L. Delle Rose, S. Khalil, S. J. D. King, and S. Moretti, R_K and R_{K^*} in an aligned 2HDM with right-handed neutrinos, *Phys. Rev. D* **101**, 115009 (2020).

- [79] L. Delle Rose, S. Khalil, and S. Moretti, Explaining electron and muon $g-2$ anomalies in an aligned 2-Higgs doublet model with right-handed neutrinos, *Phys. Lett. B* **816**, 136216 (2021).
- [80] G. Arcadi, A. S. De Jesus, T. B. De Melo, F. S. Queiroz, and Y. S. Villamizar, A 2HDM for the $g-2$ and dark matter, [arXiv:2104.04456](https://arxiv.org/abs/2104.04456).
- [81] T. Lee, A theory of spontaneous T violation, *Phys. Rev. D* **8**, 1226 (1973).
- [82] H. E. Haber and G. L. Kane, The search for supersymmetry: Probing physics beyond the standard model, *Phys. Rep.* **117**, 75 (1985).
- [83] G. Branco, P. Ferreira, L. Lavoura, M. Rebelo, M. Sher, and J. P. Silva, Theory and phenomenology of Two-Higgs-Doublet models, *Phys. Rep.* **516**, 1 (2012).
- [84] M. Tanabashi *et al.* (Particle Data Group), Review of particle physics, *Phys. Rev. D* **98**, 030001 (2018).
- [85] A. Ibarra, Reconstructing the two right-handed neutrino model, *J. High Energy Phys.* **01** (2006) 064.
- [86] M. Klasen, F. Lyonnet, and F. S. Queiroz, NLO + NLL collider bounds, Dirac fermion and scalar dark matter in the B–L model, *Eur. Phys. J. C* **77**, 348 (2017).
- [87] F. DEramo, N. Fernandez, and S. Profumo, When the universe expands too fast: Relentless dark matter, *J. Cosmol. Astropart. Phys.* **05** (2017) 012.
- [88] E. W. Kolb and M. S. Turner, *The Early Universe*, Frontiers in Physics (Westview Press, Boulder, CO, 1990).
- [89] B. Barman, P. Ghosh, F. S. Queiroz, and A. K. Saha, Scalar multiplet dark matter in a fast expanding universe: Resurrection of the desert region, *Phys. Rev. D* **104**, 015040 (2021).
- [90] P. Zyla *et al.* (Particle Data Group), Review of particle physics, *Prog. Theor. Exp. Phys.* **2020**, 083C01 (2020).
- [91] R. R. Caldwell, R. Dave, and P. J. Steinhardt, Cosmological Imprint of an Energy Component with General Equation of State, *Phys. Rev. Lett.* **80**, 1582 (1998).
- [92] V. Sahni and A. Starobinsky, The case for a positive cosmological λ -term, *Int. J. Mod. Phys. D* **09**, 373 (2000).
- [93] P. Salati, Quintessence and the relic density of neutralinos, *Phys. Lett. B* **571**, 121 (2003).
- [94] A. Kamenshchik, U. Moschella, and V. Pasquier, An alternative to quintessence, *Phys. Lett. B* **511**, 265 (2001).
- [95] H. A. Borges and P. Hepp, Growth rate in inhomogeneous interacting vacuum models (2018).
- [96] B. Ratra and P. J. E. Peebles, Cosmological consequences of a rolling homogeneous scalar field, *Phys. Rev. D* **37**, 3406 (1988).
- [97] G. Arcadi and P. Ullio, Accurate estimate of the relic density and the kinetic decoupling in nonthermal dark matter models, *Phys. Rev. D* **84**, 043520 (2011).
- [98] G. Arcadi, S. Profumo, F. Queiroz, and C. Siqueira, Right-handed neutrino dark matter, neutrino masses, and non-standard cosmology in a 2HDM, *J. Cosmol. Astropart. Phys.* **12** (2020) 030.
- [99] G. F. Giudice, E. W. Kolb, and A. Riotto, Largest temperature of the radiation era and its cosmological implications, *Phys. Rev. D* **64**, 023508 (2001).
- [100] M. Drees and F. Hajkarim, Dark matter production in an early matter dominated era, *J. Cosmol. Astropart. Phys.* **02** (2018) 057.
- [101] P. Chanda, S. Hamdan, and J. Unwin, Reviving z and Higgs mediated dark matter models in matter dominated freeze-out, *J. Cosmol. Astropart. Phys.* **01** (2020) 034.
- [102] P. Arias, N. Bernal, A. Herrera, and C. Maldonado, Reconstructing non-standard cosmologies with dark matter, *J. Cosmol. Astropart. Phys.* **10** (2019) 047.
- [103] G. L. Kane, P. Kumar, B. D. Nelson, and B. Zheng, Dark matter production mechanisms with a nonthermal cosmological history: A classification, *Phys. Rev. D* **93**, 063527 (2016).
- [104] T. Moroi and L. Randall, Wino cold dark matter from anomaly mediated susy breaking, *Nucl. Phys.* **B570**, 455 (2000).
- [105] F. De Bernardis, L. Pagano, and A. Melchiorri, New constraints on the reheating temperature of the universe after WMAP-5, *Astropart. Phys.* **30**, 192 (2008).
- [106] M. Kawasaki, K. Kohri, and N. Sugiyama, MeV-scale reheating temperature and thermalization of the neutrino background, *Phys. Rev. D* **62**, 023506 (2000).
- [107] S. Hannestad, What is the lowest possible reheating temperature? *Phys. Rev. D* **70**, 043506 (2004).
- [108] S. Hamdan and J. Unwin, Dark matter freeze-out during matter domination, *Mod. Phys. Lett. A* **33**, 1850181 (2018).
- [109] S. Hamdan, Dark matter freeze-out in a matter dominated universe, PhD thesis, Illinois University, Chicago, 2018.
- [110] G. Aad *et al.* (ATLAS Collaboration), Search for high-mass dilepton resonances using 139 fb^{-1} of pp collision data collected at $\sqrt{s} = 13 \text{ TeV}$ with the ATLAS detector, *Phys. Lett. B* **796**, 68 (2019).
- [111] A. M. Sirunyan *et al.* (CMS Collaboration), Search for low mass vector resonances decaying into quark-antiquark pairs in proton-proton collisions at $\sqrt{s} = 13 \text{ TeV}$, *Phys. Rev. D* **100**, 112007 (2019).
- [112] B. Grinstein, R. P. Springer, and M. B. Wise, Strong interaction effects in weak radiative \bar{B} meson decay, *Nucl. Phys.* **B339**, 269 (1990).
- [113] M. Misiak and M. Steinhauser, Weak radiative decays of the B meson and bounds on M_{H^\pm} in the Two-Higgs-Doublet model, *Eur. Phys. J. C* **77**, 201 (2017).
- [114] H. Davoudiasl, H.-S. Lee, and W. J. Marciano, Muon $g-2$, rare kaon decays, and parity violation from dark bosons, *Phys. Rev. D* **89**, 095006 (2014).
- [115] G. Arcadi, M. Lindner, J. Martins, and F. S. Queiroz, New physics probes: Atomic parity violation, polarized electron scattering and neutrino-nucleus coherent scattering, *Nucl. Phys.* **B959**, 115158 (2020).
- [116] A. L. Fitzpatrick, W. Haxton, E. Katz, N. Lubbers, and Y. Xu, The effective field theory of dark matter direct detection, *J. Cosmol. Astropart. Phys.* **02** (2013) 004.

-
- [117] A. L. Fitzpatrick, W. Haxton, E. Katz, N. Lubbers, and Y. Xu, Model independent direct detection analyses, [arXiv:1211.2818](#).
- [118] N. Anand, A. L. Fitzpatrick, and W. C. Haxton, Weakly interacting massive particle-nucleus elastic scattering response, *Phys. Rev. C* **89**, 065501 (2014).
- [119] M. Cirelli, E. Del Nobile, and P. Panci, Tools for model-independent bounds in direct dark matter searches, *J. Cosmol. Astropart. Phys.* **10** (2013) 019.
- [120] B. Barman, P. Ghosh, F. S. Queiroz, and A. K. Saha, Scalar multiplet dark matter in a fast expanding universe: Resurrection of the desert region, *Phys. Rev. D* **104**, 015040 (2021).